APPLIED SCIENCES AND ENGINEERING

Opto-refrigerative tweezers

Jingang Li[1], Zhihan Chen[1], Yaoran Liu[2], Pavana Siddhartha Kollipara[3], Yichao Feng[4], Zhenglong Zhang[4], Yuebing Zheng[1,2,3]*

Optical tweezers offer revolutionary opportunities for both fundamental and applied research in materials science, biology, and medical engineering. However, the requirement of a strongly focused and high-intensity laser beam results in potential photon-induced and thermal damages to target objects, including nanoparticles, cells, and biomolecules. Here, we report a new type of light-based tweezers, termed opto-refrigerative tweezers, which exploit solid-state optical refrigeration and thermophoresis to trap particles and molecules at the laser-generated cold region. While laser refrigeration can avoid photothermal heating, the use of a weakly focused laser beam can further reduce the photodamages to the target object. This novel and noninvasive optical tweezing technique will bring new possibilities in the optical control of nanomaterials and biomolecules for essential applications in nanotechnology, photonics, and life science.

INTRODUCTION

Optical tweezers were extensively applied to trap and manipulate colloidal particles and biological objects (*1*, *2*). The invention of optical tweezers has stimulated notable advances in nanotechnology (*3*, *4*), physics (*5*–*7*), and biological science (*8*, *9*). Despite this far-reaching progress, the diffraction limit makes it challenging to trap nanoscale objects using optical tweezers (*10*). Thus, a tightly focused laser beam with high optical intensity is usually required, which may cause photodamages and photothermal degradation to nanoparticles and biological samples (*11*–*13*).

A variety of strategies and techniques were proposed to overcome these limitations. Near-field optical nanotweezers exploit strong plasmon-enhanced optical forces to accurately trap nanoparticles and molecules at metallic nanoantennas (*14*, *15*) or plasmonic nanoapertures (*16*) with reduced optical power. However, the localized near-field enhancement may lead to strong plasmonic heating and limit the capability for dynamic manipulation. Alternatively, indirect optomechanical coupling under a light-controlled electric field or temperature field has been harnessed to manipulate particles and cells with low optical intensity and increased flexibility (*17*–*19*). However, the potential photothermal damages still exist, which may hinder their implementation in the research that involves fragile nanomaterials and thermosensitive biological specimens. Lately, Ndukaife and coworkers (*20*) reported opto-thermo-electrohydrodynamic tweezers to trap and manipulate sub–10-nm objects away from the laser beam to avoid phototoxicity and thermal stress.

RESULTS

Here, we develop opto-refrigerative tweezers (ORTs) to dynamically manipulate objects at a laser-generated cold spot enabled by optical refrigeration and thermophoresis synergy. The localized laser cooling of the substrate generates a nonuniform temperature gradient field in the solution, in which colloidal particles and molecules can be trapped at the low-temperature region (i.e., the laser spot) via thermophoresis (Fig. 1A). A low temperature at the trapping location eliminates photothermal damages. In addition, the general thermophobic nature permits the trapping of various colloids and biomolecules in liquid media by ORT. Localized laser cooling in liquid media was realized with ytterbium-doped yttrium lithium fluoride (Yb:YLF) crystals and a 1020-nm laser (see figs. S1 and S2 and the Supplementary Materials) (*21*, *22*). The optical refrigeration of Yb-doped crystals is realized by anti-Stokes fluorescence (*23*–*25*). Briefly, the excitation at 1020 nm is matched with the E4-E5 transition in Yb^{3+} and results in photon emission at shorter wavelengths, which leads to the internal cooling of the nanocrystals (fig. S3).

A quasi-continuous Yb:YLF layer was prepared as the substrate for the laser refrigeration and opto-refrigerative trapping experiments (fig. S4). Figure 1B shows the temperature distribution at the substrate-liquid interface under laser cooling in situ measured by a thermal camera. A localized decrease of ~7.5 K in temperature was instantly observed at the laser beam center with an irradiation intensity of 25.8 mW μm^{-2}. The simulated out-of-plane temperature distribution also revealed a confined colder region at the laser spot (Fig. 1C), indicating that a temperature gradient pointing outward from the laser beam was built in a three-dimensional way. The corresponding temperature gradient mapping is shown in Fig. 1D, where a high gradient of $>1 \times 10^7$ K m^{-1} was obtained at the periphery of the laser beam center. The optical refrigeration was further confirmed by measuring the upconversion emission from Yb/Er codoped YLF nanocrystals (fig. S5) (*26*). The power-dependent laser cooling of the substrate is shown in Fig. 1E. With an increasing incident intensity from 20 to 41 mW μm^{-2}, a temperature decrease of ~6 to 10 K was observed, and the temperature gradient increased from 0.6 to 1.4×10^7 K m^{-1} (figs. S6 to S8). Under such a strong temperature gradient field ∇T, colloidal particles or molecules experience a thermodiffusive drift velocity $v_T = -DS_T\nabla T$ (*27*, *28*), where D and S_T are the diffusion coefficient and Soret coefficient, respectively. In general, most particles and molecules exhibit a thermophobic behavior with a positive S_T, which will migrate toward the colder region in a temperature gradient (*29*, *30*). In our case, thermophoresis drives particles and molecules to the laser-generated cold spot and traps them at the laser beam center. The effective thermophoretic trapping force in a solution can be written as $F_T = \gamma v_T = -k_B T S_T \nabla T$, where γ is the friction coefficient and related to the Boltzmann

[1]Materials Science and Engineering Program and Texas Materials Institute, The University of Texas at Austin, Austin, TX 78712, USA. [2]Department of Electrical and Computer Engineering, The University of Texas at Austin, Austin, TX 78705, USA. [3]Walker Department of Mechanical Engineering, The University of Texas at Austin, Austin, TX 78712, USA. [4]School of Physics and Information Technology, Shaanxi Normal University, Xi'an, Shaanxi 710062, China.
*Corresponding author. Email: zheng@austin.utexas.edu

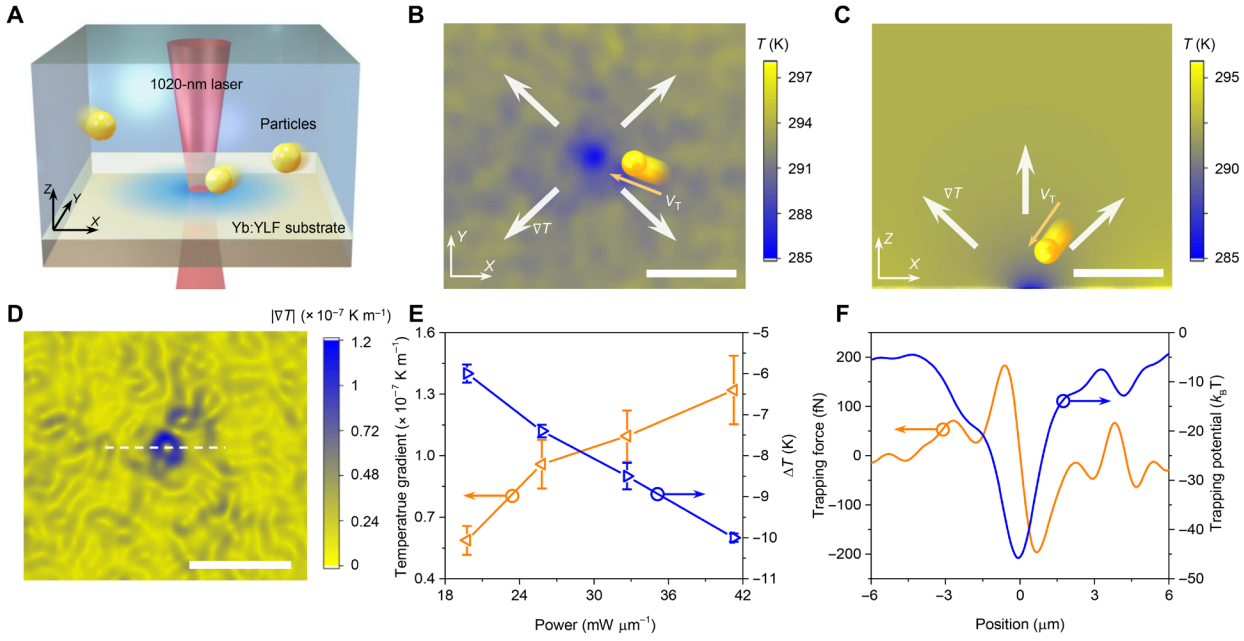

Fig. 1. Working principle of ORT. (**A**) Schematic of the localized laser cooling of Yb:YLF substrate and the thermophoretic trapping of particles at the cold spot. (**B**) Measured in-plane temperature distribution at the solution-substrate interface under a laser intensity of 25.8 mW μm^{-2}. (**C**) Simulated out-of-plane temperature distribution based on the temperature profile crossing the laser beam center in (B). (**D**) In-plane temperature gradient mapping corresponding to (B). (**E**) Power-dependent laser cooling. The average temperature drops at the laser beam center, and the peripheral temperature gradient values were plotted. (**F**) The effective thermophoretic trapping force and the trapping potential along the white dashed line in (D). A Soret coefficient of 4 K^{-1} was used. The position of the laser beam center was set to be 0. Scale bars, 10 μm.

constant k_B by Stokes-Einstein relation $\gamma D = k_B T$ (*31*). For a typical Soret coefficient of ~4 K^{-1} for colloidal nanoparticles (*30*, *32*), a maximum trapping force of ~200 fN and a trapping potential of ~45 $k_B T$ were obtained (Fig. 1F), indicating that stable trapping of nanoparticles can be achieved.

We used 200-nm fluorescent polystyrene (PS) nanoparticles to demonstrate the capability of ORT for single-particle trapping and manipulation. Heavy water (D_2O) was used as the liquid medium for ORT due to its low light absorption at 1020 nm (*21*). In addition, laser refrigeration of Yb:YLF can be extended to other media, such as H_2O (fig. S9). Figure 2A shows the attraction, trapping, and subsequent release of a PS nanoparticle. Compared with optical tweezers and plasmonic tweezers, trapping in a temperature gradient field has the advantage of a long working range (Fig. 1B) to effectively trap nanoparticles at a distance of more than 10 μm away from the laser beam. Figure 2B shows the dynamic transport of a trapped particle on the Yb:YLF substrate (see movie S1 for the trapping and manipulation). Note that optical force is much smaller than thermophoretic force in our trapping experiments (fig. S10). In addition, when the laser was moved away from the Yb:YLF substrate to the glass, the trapped nanoparticle was immediately released (movie S2 and fig. S11), indicating that thermophoretic force enabled by optical refrigeration is the main driving force in ORT.

To assess the trapping stability of ORT, we measured the trapping stiffness by tracking the trajectories of a trapped 200-nm PS nanoparticle (Fig. 2C). With the increase of optical intensity, the trapped nanoparticle became more confined to the laser beam center (fig. S12). We fitted the histograms of the particle displacement (Fig. 2D) with a Gaussian function to obtain the variance σ and extracted the trapping stiffness $\kappa = \frac{2k_B T}{\sigma^2}$ (*33*). A high trapping stiffness of 0.5 to 4 pN μm^{-1} was obtained, corresponding to a laser intensity of 20 to 41 mW μm^{-2}, which is consistent with the values calculated from temperature mapping (Fig. 2E). Our trapping stiffness is comparable with near-field trapping of a 200-nm PS nanoparticle on plasmonic nanodimers (*10*), while our optical intensity is one order of magnitude lower. We note that the theoretical trapping stiffness based on the temperature gradient profiles is slightly smaller than the experimental results extracted from the particle tracking; this discrepancy is probably caused by the limited spatial resolution in the temperature measurement.

Besides providing a general platform to trap nanoparticles and molecules with thermophobic nature based on thermophoresis, ORT stands out for research in colloidal sciences and biology due to the capability to trap and manipulate objects with low damages. Compared to optical tweezers, ORT relies on a temperature gradient field to trap the target objects. Therefore, a weakly focused laser beam [numerical aperture (NA) = 0.5 to 0.7] with lower intensity was used to remarkably reduce the photodamages. Meanwhile, the intrinsic feature of trapping objects at the cold region avoids the common photothermal heating and the resultant thermal degradation in other optical tweezing platforms. As a demonstration, we compared the quenching of a 200-nm fluorescent PS nanoparticle trapped by ORT and optical tweezers (Fig. 3A). The same 1020-nm laser was used in both ORT and optical tweezers for the trapping experiments. For conventional optical tweezers, the PS particle exhibited a marked drop in the fluorescence intensity, while the PS particle trapped by ORT only showed a slight decrease (Fig. 3B). The fluorescence intensity decreased to ~65% for optical tweezers and remained at >90% for ORT (Fig. 3C). This enhanced stability of trapped objects is attributed to the suppression of both photobleaching and thermal bleaching in ORT (*34*).

In addition to dye-doped nanoparticles, most biomolecules are sensitive to environmental temperature. For example, many proteins

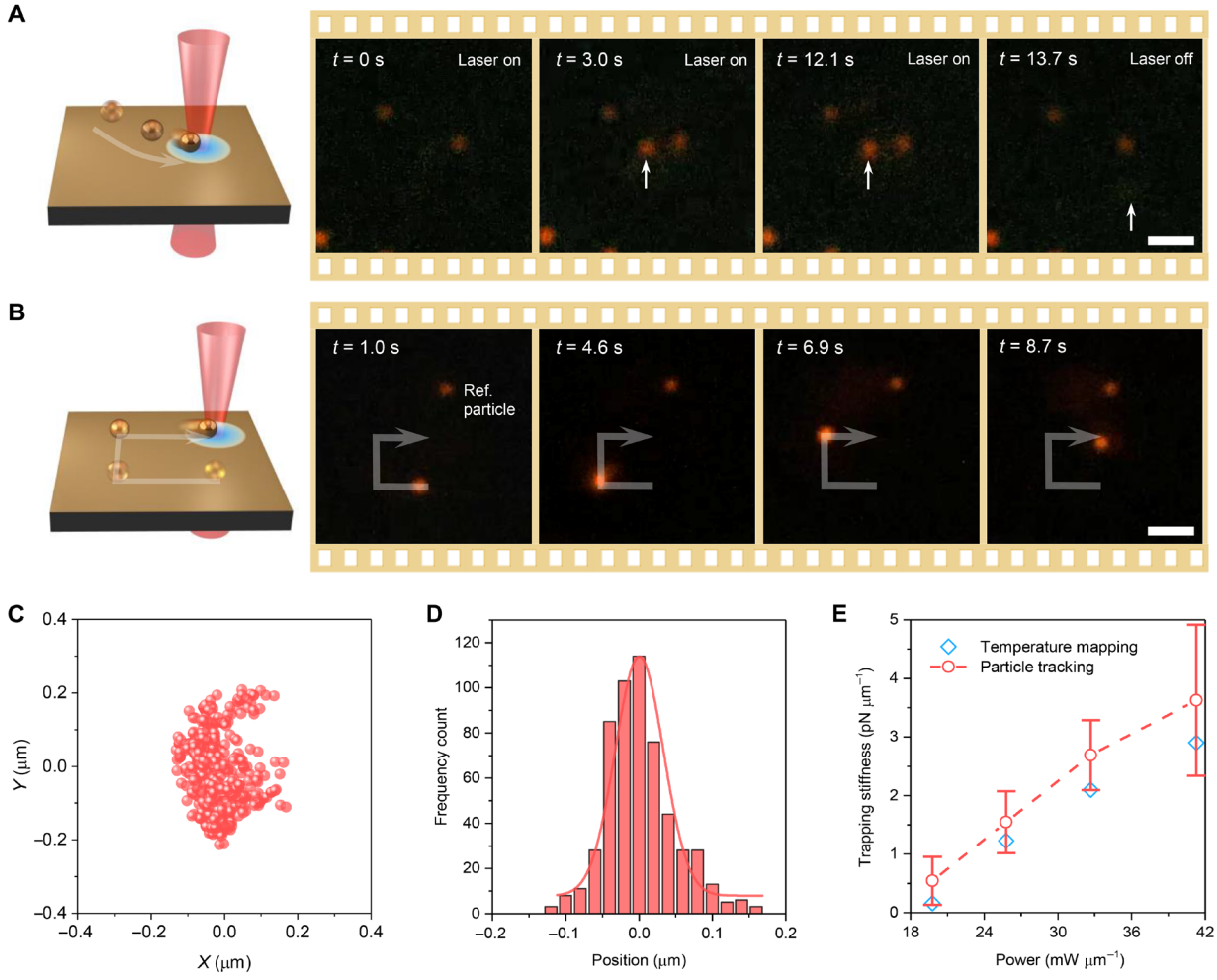

Fig. 2. Trapping and manipulating single nanoparticles with ORT. (**A**) Trapping and releasing a 200-nm PS nanoparticle. (**B**) Dynamic manipulation of a 200-nm PS nanoparticle. The white arrows indicate the position and the trajectory of the particle, respectively. Laser intensity of ~25 mW μm^{-2}. (**C**) A typical position distribution of a 200-nm PS nanoparticle trapped by ORT with an optical intensity of 20 mW μm^{-2}. (**D**) Histogram of particle displacement (*x* direction) corresponding to (C). (**E**) Power-dependent trapping stiffness of a 200-nm PS nanoparticle trapped by ORT. Both experimental trapping stiffness from particle tracking and theoretical trapping stiffness from temperature mapping are plotted. Scale bars, 5 μm.

and RNA molecules are subject to thermal degradation at high or even ambient temperature (*35*, *36*). Therefore, ORT offers the new possibility to trap these biomolecules and simultaneously cool down their environmental temperature (ΔT > 10 K), which substantially enhances the stability of thermosensitive molecules. A proof-of-concept demonstration is presented in Fig. 3 (D and E), where fluorescein isothiocyanate (FITC)–conjugated protein A/G was trapped and concentrated at the laser-generated cold spot via ORT. This non-invasive optical concentration of biomolecules is promising in studying molecular interactions for disease diagnosis and drug development (*37*, *38*).

DISCUSSION

In summary, we developed ORTs through the innovative coordination of optical refrigeration and thermophoresis. It presents a new type of optical tweezing tool that enables the trapping of objects in the low-temperature region to avoid photothermal damages. Since it is based on a temperature gradient field, ORT allows the long-range trapping with a low-intensity and weakly focused laser beam, which can reduce the photon degradation of target objects.

The common thermophobic nature and positive Soret coefficients make ORT a general manipulation tool for nanoparticles and molecules of a broad range of compositions. However, note that negative Soret coefficients can be observed in certain circumstances, where ORT is not applicable. For instance, the presence of surfactants in the solution can alter the thermophoretic response of colloidal particles (*39*). Currently, the substrate, i.e., Yb:YLF nanoparticle layer, is prepared by a simple drop-cast method. Alternative approaches such as doctor blade coating (*40*) can be applied to improve the surface uniformity of the substrate. In addition, the large width of trapping potential may lead to the trapping of multiple particles when the particle concentration is high. One possible way to ensure the capability to trap single objects is to design a narrow trapping potential that is comparable to the size of the target particle by using a single Yb:YLF nanocrystal as the cooling substrate.

As a newly developed technique, ORT still has several limitations and future efforts that can be made to further enhance its strengths.

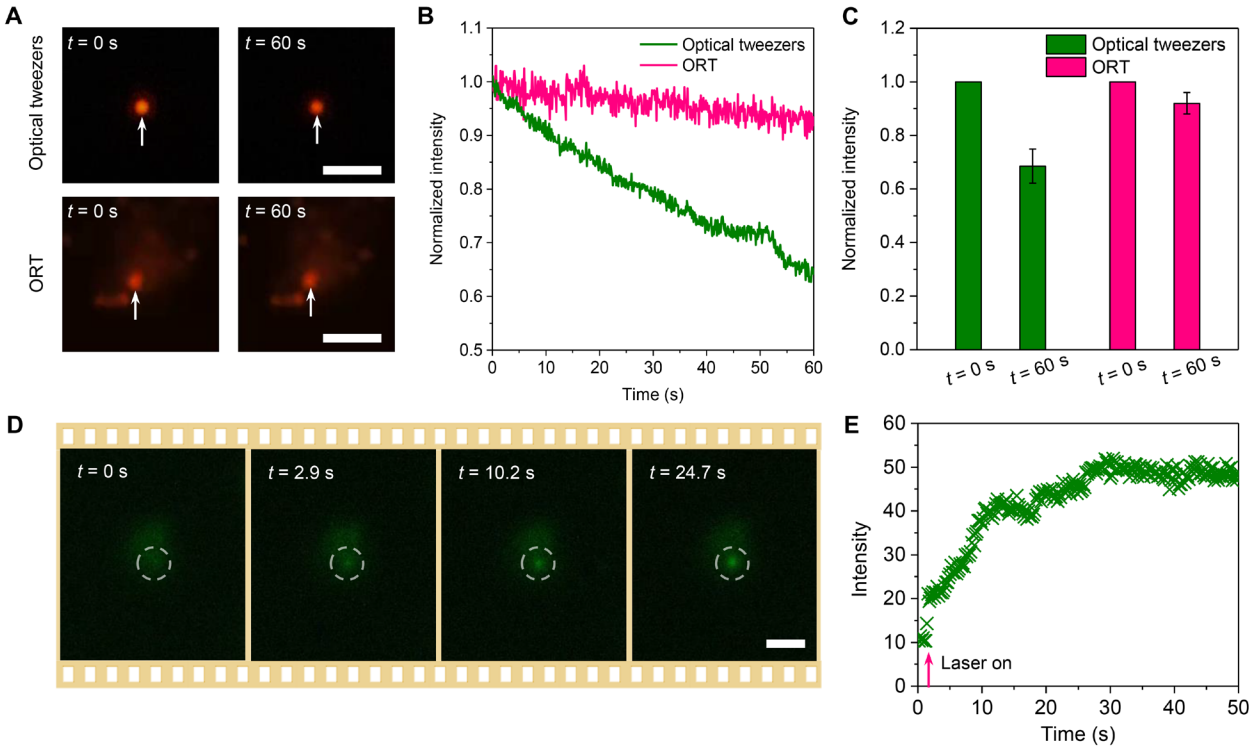

Fig. 3. Noninvasive trapping of nanoparticles and biomolecules with ORT. (**A**) Optical images of a single 200-nm PS nanoparticle before and after being trapped by optical tweezers (top) and ORT (bottom) for 1 min. (**B**) Time-resolved fluorescence intensity of the PS particle trapped by optical tweezers and ORT. (**C**) Normalized fluorescence intensity changes after the PS particle was trapped for 1 min. (**D**) Successive optical images showing the trapping and concentration of FITC-conjugated protein A/G. (**E**) Time resolve intensity at the laser spot during the concentration of FITC-conjugated protein A/G. Scale bars, 5 μm.

With the capability of stable trapping, dynamic manipulation, and noninvasive operation, ORT will serve as a powerful nanotool to open new opportunities for many fields, including materials science, physical chemistry, and biological science.

MATERIALS AND METHODS

Chemicals

$Y(NO_3)_3$, $Yb(NO_3)_3$, and $Er(NO_3)_3$ (all in 99.9%) and deuterium oxide (D_2O; 99.9 atom % D) were purchased from Sigma-Aldrich. Lithium fluoride (LiF; 98.0%), ammonium fluoride (NH_4F; 98.0%), and EDTA (99.0%) were supplied by Sinopharm Chemical Reagent Co. Ltd. Fluorescent dye–doped PS nanoparticles (with suncoast yellow and dragon green) were purchased from Bangs Laboratories Inc. FITC-conjugated protein A/G (FITC-protein A/G) was bought from BioVision.

Synthesis of Yb:YLF crystals

Yb^{3+}-doped $LiYF_4$ crystals were synthesized by a previously reported hydrothermal method (*41*). In this work, 10% Yb^{3+}:$LiYF_4$ was used. First, 0.1 ml of $Yb(NO_3)_3$ (0.5 M), 0.9 ml of $Y(NO_3)_3$ (0.5 M), and 0.93 g of EDTA were added in a 20.0 ml of deionized (DI) water and stirred for 30 min to form a chelate complex solution. Then, 0.17 g of NH_4F and 0.48 g of LiF were added, and the solution was stirred for ~20 min until it became a white liquid completely. Next, this white liquid was transferred into a 40-ml Teflon-lined autoclave and heated at 220°C for 48 hours. The obtained white powders were centrifuged and washed with DI water and ethanol three times. The collected powders were lastly dried at 60°C for 12 hours. To synthesize the $Yb^{3+}$and Er^{3+} codoped $LiYF_4$ crystals, $Y(NO_3)_3$ was replaced with a precursor mixture containing 2% of $Er(NO_3)_3$ under the same reaction conditions.

Sample preparation

The as-synthesized Yb:YLF crystals with a length of 10 to 15 μm were transferred into a mortar and ground to fine crystals with a size of ~1 to 2 μm. The fine crystals were stored in ethanol, and the size was check with scanning electron microscopy (SEM). Quasi-continuous Yb:YLF substrates were prepared by drop-casting 5 μl of Yb:YLF crystal solution on the glass, drying it under room temperature, and washing it with DI water and ethanol several times. Quasi-continuous Yb:YLF substrate with a typical size larger than 100 μm was easy to be obtained for the trapping and manipulation experiments. Reproducible quasi-continuous particle layers were obtained by controlling the particle concentration and droplet size. All trapping and manipulation experiments with ORT were performed in heavy water (D_2O); control experiments with conventional optical tweezers were conducted in DI water with the same setup, except that a high NA of 1 to 1.3 was used to create enough trapping forces for the nanoparticles.

Characterizations

The crystal structure was characterized by a D/Max2550VB+/PC x-ray diffraction meter. The morphology, size, and composition were

measured with an SEM (FEI Quanta FEG 650 SEM). The photoluminescence spectra from the nanocrystals were measured with a spectrometer from Andor Technology. The integrated emission in fig. S5 was obtained by calculating the integration area of the photoluminescence spectra by an Origin software.

Temperature measurement

The in situ and real-time microscale temperature profiles were measured with a thermal camera (SID4-HR, Phasics) and a temperature imaging by quadriwave shearing interferometry technique. A reference temperature mapping was first recorded when the laser is off. Then, the temperature mapping data were measured immediately after the laser is turned on. Twenty images were taken to obtain the average temperature mapping profile in one measurement to reduce the noise. SIDFTHERMO software (Phasics) was used to record and analyze the temperature profiles. A MATLAB code was further applied to smooth the temperature mapping to remove the noise.

Numerical simulations

The temperature profiles were simulated using COMSOL based on the measured temperature profiles and the thermal conductivity of heavy water. The outer boundary was set at the room temperature. Optical forces were simulated using the finite-difference time-domain method (Lumerical). The mesh size was set to 2 nm for nanoparticles.

SUPPLEMENTARY MATERIALS

Supplementary material for this article is available at http://advances.sciencemag.org/cgi/content/full/7/26/eabh1101/DC1

REFERENCES AND NOTES

1. D. G. Grier, A revolution in optical manipulation. *Nature* **424**, 810–816 (2003).
2. A. Ashkin, J. M. Dziedzic, T. Yamane, Optical trapping and manipulation of single cells using infrared laser beams. *Nature* **330**, 769–771 (1987).
3. O. M. Maragò, P. H. Jones, P. G. Gucciardi, G. Volpe, A. C. Ferrari, Optical trapping and manipulation of nanostructures. *Nat. Nanotechnol.* **8**, 807–819 (2013).
4. E. McLeod, C. B. Arnold, Subwavelength direct-write nanopatterning using optically trapped microspheres. *Nat. Nanotechnol.* **3**, 413–417 (2008).
5. T. L. Gustavson, A. P. Chikkatur, A. E. Leanhardt, A. Görlitz, S. Gupta, D. E. Pritchard, W. Ketterle, Transport of Bose-Einstein condensates with optical tweezers. *Phys. Rev. Lett.* **88**, 020401 (2001).
6. F. Han, J. A. Parker, Y. Yifat, C. Peterson, S. K. Gray, N. F. Scherer, Z. Yan, Crossover from positive to negative optical torque in mesoscale optical matter. *Nat. Commun.* **9**, 4897 (2018).
7. Z. Yan, M. Sajjan, N. F. Scherer, Fabrication of a material assembly of silver nanoparticles using the phase gradients of optical tweezers. *Phys. Rev. Lett.* **114**, 143901 (2015).
8. A. Ashkin, J. M. Dziedzic, Optical trapping and manipulation of viruses and bacteria. *Science* **235**, 1517–1520 (1987).
9. J. R. Moffitt, Y. R. Chemla, S. B. Smith, C. Bustamante, Recent advances in optical tweezers. *Annu. Rev. Biochem.* **77**, 205–228 (2008).
10. A. N. Grigorenko, N. W. Roberts, M. R. Dickinson, Y. Zhang, Nanometric optical tweezers based on nanostructured substrates. *Nat. Photonics* **2**, 365–370 (2008).
11. A. Blázquez-Castro, Optical tweezers: Phototoxicity and thermal stress in cells and biomolecules. *Micromachines* **10**, 507 (2019).
12. A. Babynina, M. Fedoruk, P. Kühler, A. Meledin, M. Döblinger, T. Lohmüller, Bending gold nanorods with light. *Nano Lett.* **16**, 6485–6490 (2016).
13. M. B. Rasmussen, L. B. Oddershede, H. Siegumfeldt, Optical tweezers cause physiological damage to *Escherichia coli* and *Listeria* bacteria. *Appl. Environ. Microbiol.* **74**, 2441–2446 (2008).
14. M. L. Juan, M. Righini, R. Quidant, Plasmon nano-optical tweezers. *Nat. Photonics* **5**, 349–356 (2011).
15. J. C. Ndukaife, A. V. Kildishev, A. G. A. Nnanna, V. M. Shalaev, S. T. Wereley, A. Boltasseva, Long-range and rapid transport of individual nano-objects by a hybrid electrothermoplasmonic nanotweezer. *Nat. Nanotechnol.* **11**, 53–59 (2015).
16. A. Kotnala, R. Gordon, Quantification of high-efficiency trapping of nanoparticles in a double nanohole optical tweezer. *Nano Lett.* **14**, 853–856 (2014).
17. P. Y. Chiou, A. T. Ohta, M. C. Wu, Massively parallel manipulation of single cells and microparticles using optical images. *Nature* **436**, 370–372 (2005).
18. L. Lin, M. Wang, X. Peng, E. N. Lissek, Z. Mao, L. Scarabelli, E. Adkins, S. Coskun, H. E. Unalan, B. A. Korgel, L. M. Liz-Marzán, E.-L. Florin, Y. Zheng, Opto-thermoelectric nanotweezers. *Nat. Photonics* **12**, 195–201 (2018).
19. Y. Liu, L. Lin, B. Bangalore Rajeeva, J. W. Jarrett, X. Li, X. Peng, P. Kollipara, K. Yao, D. Akinwande, A. K. Dunn, Y. Zheng, Nanoradiator-mediated deterministic opto-thermoelectric manipulation. *ACS Nano* **12**, 10383–10392 (2018).
20. C. Hong, S. Yang, J. C. Ndukaife, Stand-off trapping and manipulation of sub-10 nm objects and biomolecules using opto-thermo-electrohydrodynamic tweezers. *Nat. Nanotechnol.* **15**, 908–913 (2020).
21. P. B. Roder, B. E. Smith, X. Zhou, M. J. Crane, P. J. Pauzauskie, Laser refrigeration of hydrothermal nanocrystals in physiological media. *Proc. Natl. Acad. Sci. U.S.A.* **112**, 15024–15029 (2015).
22. X. Zhou, B. E. Smith, P. B. Roder, P. J. Pauzauskie, Laser refrigeration of ytterbium-doped sodium–yttrium–fluoride nanowires. *Adv. Mater.* **28**, 8658–8662 (2016).
23. D. V. Seletskiy, S. D. Melgaard, S. Bigotta, A. di Lieto, M. Tonelli, M. Sheik-Bahae, Laser cooling of solids to cryogenic temperatures. *Nat. Photonics* **4**, 161–164 (2010).
24. A. T. M. A. Rahman, P. F. Barker, Laser refrigeration, alignment and rotation of levitated Yb^{3+}:YLF nanocrystals. *Nat. Photonics* **11**, 634–638 (2017).
25. J. Zhang, D. Li, R. Chen, Q. Xiong, Laser cooling of a semiconductor by 40 kelvin. *Nature* **493**, 504–508 (2013).
26. F. Vetrone, R. Naccache, A. Zamarrón, A. Juarranz de la Fuente, F. Sanz-Rodríguez, L. Martinez Maestro, E. Martín Rodriguez, D. Jaque, J. García Solé, J. A. Capobianco, Temperature sensing using fluorescent nanothermometers. *ACS Nano* **4**, 3254–3258 (2010).
27. A. Würger, Thermal non-equilibrium transport in colloids. *Rep. Prog. Phys.* **73**, 126601 (2010).
28. S. Duhr, D. Braun, Why molecules move along a temperature gradient. *Proc. Natl. Acad. Sci. U.S.A.* **103**, 19678–19682 (2006).
29. M. Braun, A. P. Bregulla, K. Günther, M. Mertig, F. Cichos, Single molecules trapped by dynamic inhomogeneous temperature fields. *Nano Lett.* **15**, 5499–5505 (2015).
30. M. Braun, F. Cichos, Optically controlled thermophoretic trapping of single nano-objects. *ACS Nano* **7**, 11200–11208 (2013).
31. J. Burelbach, M. Zupkauskas, R. Lamboll, Y. Lan, E. Eiser, Colloidal motion under the action of a thermophoretic force. *J. Chem. Phys.* **147**, 094906 (2017).
32. Y. T. Maeda, A. Buguin, A. Libchaber, Thermal separation: Interplay between the Soret effect and entropic force gradient. *Phys. Rev. Lett.* **107**, 038301 (2011).
33. E.-L. Florin, A. Pralle, E. H. K. Stelzer, J. K. H. Hörber, Photonic force microscope calibration by thermal noise analysis. *Appl. Phys. A* **66**, S75–S78 (1998).
34. G. Chirico, F. Cannone, G. Baldini, A. Diaspro, Two-photon thermal bleaching of single fluorescent molecules. *Biophys. J.* **84**, 588–598 (2003).
35. B. W. Matthews, H. Nicholson, W. J. Becktel, Enhanced protein thermostability from site-directed mutations that decrease the entropy of unfolding. *Proc. Natl. Acad. Sci. U.S.A.* **84**, 6663–6667 (1987).
36. G. Lee, M. A. Bratkowski, F. Ding, A. Ke, T. Ha, Elastic coupling between RNA degradation and unwinding by an exoribonuclease. *Science* **336**, 1726–1729 (2012).
37. C. Liu, J. Zhao, F. Tian, L. Cai, W. Zhang, Q. Feng, J. Chang, F. Wan, Y. Yang, B. Dai, Y. Cong, B. Ding, J. Sun, W. Tan, Low-cost thermophoretic profiling of extracellular-vesicle surface proteins for the early detection and classification of cancers. *Nat. Biomed. Eng.* **3**, 183–193 (2019).
38. C. J. Wienken, P. Baaske, U. Rothbauer, D. Braun, S. Duhr, Protein-binding assays in biological liquids using microscale thermophoresis. *Nat. Commun.* **1**, 100 (2010).
39. Q. Jiang, B. Rogez, J.-B. Claude, G. Baffou, J. Wenger, Quantifying the role of the surfactant and the thermophoretic force in plasmonic nano-optical trapping. *Nano Lett.* **20**, 8811–8817 (2020).
40. H. Yang, P. Jiang, Large-scale colloidal self-assembly by doctor blade coating. *Langmuir* **26**, 13173–13182 (2010).
41. W. Gao, J. Dong, Z. Wang, Z. Zhang, H. Zheng, Multicolor upconversion emission of lanthanide-doped single $LiYF_4$ and $LiLuF_4$ microcrystal. *Mater. Res. Bull.* **91**, 77–84 (2017).

Acknowledgments

Funding: J.L, Z.C., Y.L., P.S.K., and Y.Z. acknowledge the financial supports of the National Institute of General Medical Sciences of the National Institutes of Health (DP2GM128446) and the National Science Foundation (NSF-ECCS-2001650). J.L. also acknowledges the financial support of University Graduate Continuing Fellowship from The University of Texas at Austin.
Author contributions: J.L. and Y.Z. conceived the idea. J.L. and Z.C. prepared the samples,

worked on the experiments, and collected the data. Y.L. and P.S.K. conducted the simulations and assisted with the experimental setup. Y.F. and Z.Z. synthesized the doped YLF crystals. Y.Z. supervised the project. J.L. and Y.Z. wrote the manuscript with inputs from all authors.
Competing interests: The authors declare that they have no competing interests. **Data and materials availability:** All data needed to evaluate the conclusions in the paper are present in the paper and/or the Supplementary Materials. Additional data related to this paper may be requested from the authors.

Submitted 16 February 2021
Accepted 12 May 2021
Published 25 June 2021
10.1126/sciadv.abh1101

Citation: J. Li, Z. Chen, Y. Liu, P. S. Kollipara, Y. Feng, Z. Zhang, Y. Zheng, Opto-refrigerative tweezers. *Sci. Adv.* **7**, eabh1101 (2021).